Plasticity and adaptation to high light intensity amplify the advantage of amphistomous leaves

Christopher D. Muir[1,2*] Wei Shen Lim[1] Dachuan Wang[1,2]

[1]School of Life Sciences, University of Hawai'i, Mānoa, Hawai'i, USA
[2]Department of Botany, University of Wisconsin, Madison, Wisconsin, USA

*Corresponding author: cdmuir@wisc.edu

ORCID: Christopher D. Muir — 0000-0003-2555-3878

Abstract

The presence of stomata on both leaf surfaces (amphistomy) can increase photosynthesis in C_3 plants by reducing the path length for CO_2 diffusion between substomatal cavities and chloroplasts. Amphistomatous leaves are common among herbaceous plants growing in sunny habitats, including many crop species. This distribution of amphistomatous leaves in nature may result from an increased photosynthetic benefit of amphistomy under high light intensity, either because of acclimatory, plastic, or constitutive variation in CO_2 supply or demand. We used a recently developed method to quantify amphistomy advantage, the photosynthetic rate of an amphistomatous leaf relative to an otherwise identical hypostomatous leaf, in 29 diverse populations representing 14 species of wild tomatoes (*Solanum* sect. *Lycopersicon* and sect. *Lycopersicoides*). Plants grown under high light intensity benefit more in terms of CO_2 assimilated for a given stomatal conductance than plants grown under low light, regardless of measurement light intensity. Furthermore, populations native to open habitats tend to benefit more from amphistomy compared to those from more closed habitats. Developmental plasticity and adaptation of leaves to high light intensity likely play a combined role in explaining the adaptive significance and distribution of amphistomy in nature. We estimate that hypostomatous leaves would expend 10-65% more water to achieve the same photosynthetic rate as a comparable amphistomatous leaf, implying large fitness costs of amphistomy in ecological contexts where this trait is rare.

Main text

Stomata are microscopic pores on the surfaces of leaves and other photosynthetic organs formed by a pair of guard cells. They are essential for balancing carbon gained per unit water lost and were an

essential innovation in vascular plants, permitting them to grow tall on land by enabling access to CO_2 for photosynthetic carbon assimilation while preventing hydraulic failure in variable environments (*1–3*). Optimal stomatal function depends on both dynamic changes in aperture on the scale of minutes to hours, as well as static anatomy determined by developmental plasticity and constitutive genetic differences (*4–6*). Understanding how stomata respond to environmental change over daily, developmental, and evolutionary time is important for understanding adaptation (*1*, *7–12*), predicting paleoclimate from fossil cuticles (*13–15*), and improving crops (*16*). Stomatal function contributes to global carbon and water cycles (*17*) and therefore predicting future climate (*18*).

Despite extensive theoretical and empirical progress understanding stomata function and anatomy from molecular to ecosystem levels, the adaptive significance of amphistomatous leaves remains an important unsolved problem in leaf structure-function relationships (*19–26*). Amphistomatous leaves develop abaxial and adaxial stomata whose aperture can be independently regulated (*27–31*) to control gas exchange through each surface. All else being equal, simultaneous gas exchange through stomata on both surfaces increases CO_2 supply to chloroplasts by providing a second parallel pathway through leaf intercellular airspaces, enhancing photosynthesis (*20*, *32*). The extent to which amphistomy increases CO_2 supply depends on resistance to diffusion in intercellular airspaces. This resistance can be low in thin, porous, amphistomatous leaves (*28*, *33*), but may be more substantial in thick, dense, hypostomatous leaves (*34*). We refer to the intercellular airspace conductance (g_{ias}), the inverse of resistance. Amphistomatous leaves also lose more water through evaporation because of a second boundary layer conductance (*35*), but the additional carbon gain should be enough to offset this cost in most realistic scenarios (*36*).

The paradoxical fact is that, despite the photosynthetic benefit, most leaves are not amphistomatous. Many vertically oriented and/or isobilateral leaves are amphistomatous (*25*). But among dorsiventral leaves, it is primarily herbaceous plants in open, high light habitats that tend to have amphistomatous leaves (*22*, *39–44*). Most other leaves, except those from aquatic habitats, are hypostomatous, producing stomata only on the lower, abaxial surface. Even resupinate leaves develop stomata on the lower, albeit adaxial surface (*45*), suggesting that leaf orientation (lower vs. upper) rather than leaf polarity (abaxial vs. adaxial) is causal. The covariation between stomatal density ratio and light habitat is both qualitative and quantitative. A higher proportion of sun leaves are amphistomatous (*39*) and the proportion of stomata on the upper, adaxial surface increases with light (*42*, *43*). Resolving why high light intensity favors amphistomatous dorsivental leaves is an important first step toward understanding variation in stomatal density ratio and leaf structure-function relationships more generally.

The overarching hypothesis is that leaves with greater stomatal density ratio are more common in open, sunny habitats because they increase photosynthesis most in those circumstances. An amphistomatous leaf increases photosynthetic carbon gain compared to an otherwise identical hypostomatous leaf by increasing conductance through the leaf intercellular airspaces and boundary layers. We quantify this benefit as the amphistomy advantage (AA), the log-response ratio of photosynthesis in an amphistomatous leaf compared to an otherwise identical pseudohypostomatous leaf (*20*, *46*). Why would AA be greater in sun than shade? We consider three nonmutually exclusive hypotheses that we classify as ‘acclimation’, ‘plasticity’, and ‘constitutive’ (Fig. 1).

Table 1: Three nonmutually exclusive hypotheses and directional predictions explaining why amphistomy advantage (AA) might be greater for leaves in sunny, open habitats. For each hypothesis, we make predictions for how measurement light intensity (PPFD $= 150\,\mu\text{mol}\,\text{m}^{-2}\,\text{s}^{-1}$ vs. $2000\,\mu\text{mol}\,\text{m}^{-2}\,\text{s}^{-1}$), growth light intensity (sun vs. shade), and native plant area index (PAI) would affect AA. PPFD: photosynthetic photon flux density.

Hypothesis	Measurement light intensity	Growth light intensity	Native PAI
acclimation	$\text{AA}_{2000} > \text{AA}_{150}$	$\text{AA}_{\text{sun}} = \text{AA}_{\text{shade}}$	$\text{cor}(\text{PAI}, \text{AA}) = 0$
plastic	$\text{AA}_{2000} = \text{AA}_{150}$	$\text{AA}_{\text{sun}} > \text{AA}_{\text{shade}}$	$\text{cor}(\text{PAI}, \text{AA}) = 0$
constitutive	$\text{AA}_{2000} = \text{AA}_{150}$	$\text{AA}_{\text{sun}} = \text{AA}_{\text{shade}}$	$\text{cor}(\text{PAI}, \text{AA}) > 0$

Acclimation hypothesis: Photosynthetic induction to high light intensity typically involves increases in total leaf stomatal conductance (increased CO_2 supply), the concentration of active Rubisco, and electron transport capacity (increased CO_2 demand). If the acclimation hypothesis is correct, we predict that $\text{AA}_{2000} > \text{AA}_{150}$ for all populations regardless of native habitat or growth environment.

Plasticity hypothesis: Individuals of the same genotype often develop dramatically different leaves in sun and shade conditions (*47*). Plastic responses are likely adaptations to optimize photosynthesis at different light intensities in variable environments (*48*). Plastic changes in leaf anatomy and biochemistry could modulate AA as a byproduct. Thicker or less porous leaves, both of which are associated with high leaf mass per area (LMA), will have lower g_{ias}; leaves with increased total stomatal density and photosynthetic capacity have greater potential CO_2 supply and demand. Under the plasticity hypothesis, we predict that $\text{AA}_{\text{sun}} > \text{AA}_{\text{shade}}$ for all populations and light intensities.

Constitutive hypothesis: In environments that are relatively constant or where environmental change cannot be anticipated by a reliable cue, natural selection will favor constitutive expression of optimal phenotypes. We therefore predict genotypes from more sunny, open habitats will have consistently greater AA under all measurement and growth light intensities. For herbaceous plants, light intensity is largely a function of the tree canopy (*49*). Herbs growing in the open will regularly experience high light intensity; herbs growing under a forest canopy will often experience low light intensity.

The primary directional predictions for each hypothesis are summarized in Table 1; detailed predictions for results that would indicate simultaneous support for multiple hypotheses are in Table S3.

We tested these hypotheses by comparing AA among amphistomatous wild tomato species (Table S1; Figure S2; (*50*)) from different native light habitats, grown under simulated sun and shade light treatments, and measured under contrasting light intensities (low and high). We measured AA on 572 individual plants from 29 populations (average of 9.86 replicates per light treatment) using a recently developed method (*46*). With this method, we directly compare the photosynthetic rate of an untreated amphistomatous leaf to that of the same leaf with gas exchange blocked through the adaxial (upper) surface by transparent plastic, which we refer to as 'pseudohypostomy'. To compare amphi- and pseudohypostomatous leaves at identical whole-leaf stomatal conductance (g_{sw}), we measure A

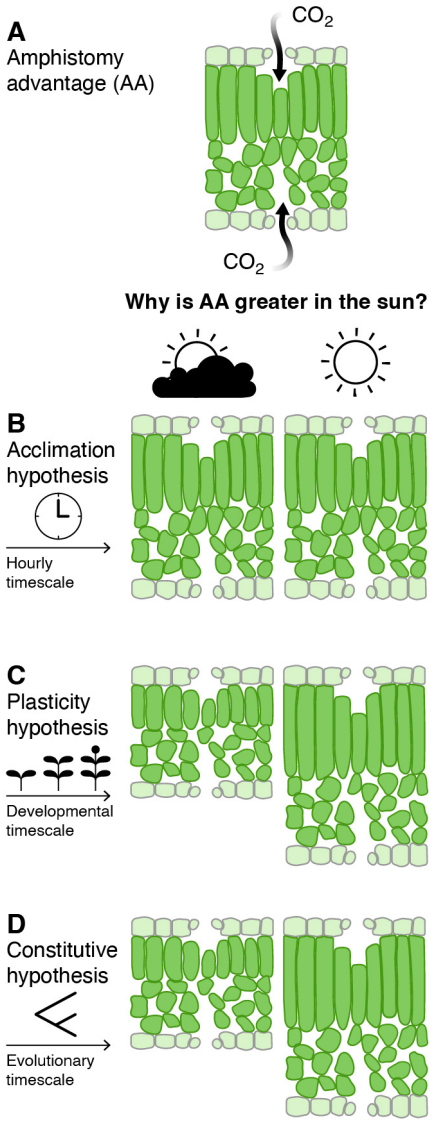

Figure 1: **Conceptual outline of three nonmutually exclusive hypotheses explaining why amphistomy advantage (AA) might be greater for leaves in sunny, open habitats.** The acclimatory hypothesis predicts that AA is greater under high measurement light intensity ($2000\,\mu mol\,m^{-2}\,s^{-1}$) than low measurement light intensity (PPFD $=$ $150\,\mu mol\,m^{-2}\,s^{-1}$), regardless of growth light intensity or native plant area index (PAI). The plasticity hypothesis predicts that AA is greater for plants grown in sun than shade, regardless of measurement light intensity or native PAI. The constitutive hypothesis predicts that AA is greater for plants adapted to sunny habitats (lower native PAI) than shaded habitats, regardless of measurement light intensity or growth light intensity.

over a range of g_{sw}, inducing stomatal opening and closure by modulating humidity (see Materials and Methods for further details). We estimated 'amphistomy advantage' (AA) *sensu* (*20*), but with modifications previously described in (*46*) and here (Materials and Methods). The native light intensity was represented by plant area index (PAI $m^2\ m^{-2}$), estimated using a global gridded data set derived from the Global Ecosystem Dynamics Investigation [GEDI; (*51*)] and georeferenced accession collection information from the Tomato Genetics Resource Center (Table S1). The growth light intensities were PPFD $=$ 761 µmol $m^{-2}\ s^{-1}$ (sun treatment) and 115 µmol $m^{-2}\ s^{-1}$ (shade treatment) while all other environment conditions were nearly identical (see Materials and Methods). The high and low measurement light intensities were PPFD $=$ 2000 µmol $m^{-2}\ s^{-1}$ (97.8:2.24 red:blue) and PPFD $=$ 150 µmol $m^{-2}\ s^{-1}$ (87.0:13.0 red:blue), respectively.

Consistent with biophysical theory of CO_2 diffusion within leaves, AA $>$ 0 for all populations (Fig. 2A). Bayesian phylogenetic mixed effects models that allowed AA to vary between measurement light intensities, growth light intensities, and among populations outperformed simpler models based on information criteria (Table S6). Measured under high light intensity, AA was consistently greater for sun plants. The average AA among populations in the shade treatment was 0.041 (range: 0.007–0.113; 19 of 29 populations significant); however, the same populations grown at high light intensity showed a mean AA of 0.052 (range: 0.020–0.120; 20 of 29 populations significant). Contrary to the predictions of the acclimation hypothesis, AA was greater in all populations under low measurement light intensity for both sun and shade grown plants. The overall average AA of shade and sun grown plants measured under low light intensity was 0.064 (range: 0.022–0.137; 28 of 29 populations significant) and 0.100 (range: 0.049–0.206; 27 of 29 populations significant), respectively. There was a modest tendency for populations from more open habitats (lower PAI) to exhibit greater AA and the slope was significantly different than 0 in 3 of the 4 treatment combinations (Fig. 2B).

The pattern of AA across wild tomatoes strongly supports the plasticity hypothesis, contradicts the acclimation hypothesis, and provides modest support for the constitutive hypothesis. Plastic changes in leaf thickness and/or packing density, summarized by the bulk leaf mass per area (LMA), may mediate the effect of growth light intensity on AA. LMA increased in sun grown plants in all populations by an average of 123% [95% CI: 42.9 to 256%], qualitatively similar to plastic responses in many species (*47*). While LMA is weakly, albeit significantly (Table S5), associated with individual-level AA (Fig. 3), the effect of growth light intensity on AA is still predictive based on model comparison (Table S6). However, the direct effect of the sun treatment on AA was weaker when LMA was included in the model (Table S4 vs. Table S5), suggestive of a mediating role. Many anatomical traits underlie LMA (*52*) and future research will be needed identify which particular traits, such as leaf thickness or mesophyll porosity, are responsible for mediating AA. The fact that the AA of sun plants was greater under low measurement light intensity supports a long-standing hypothesis that resistance to CO_2 diffusion is greater in the upper than lower portions of the leaf interior (*53*). At low light intensity, the bulk properties of the leaf are weighed toward the upper palisade where most light is intercepted. Hence, amphistomy may, unexpectedly, be particularly beneficial for sun leaves experiencing intermittent shade or cloud cover. Our study is limited in testing this because we could not directly measure the stomatal conductance ratio and intercellular resistance on each surface. Future experiments measuring AA with a dual sided chamber (*31*, *33*) can overcome these limitations.

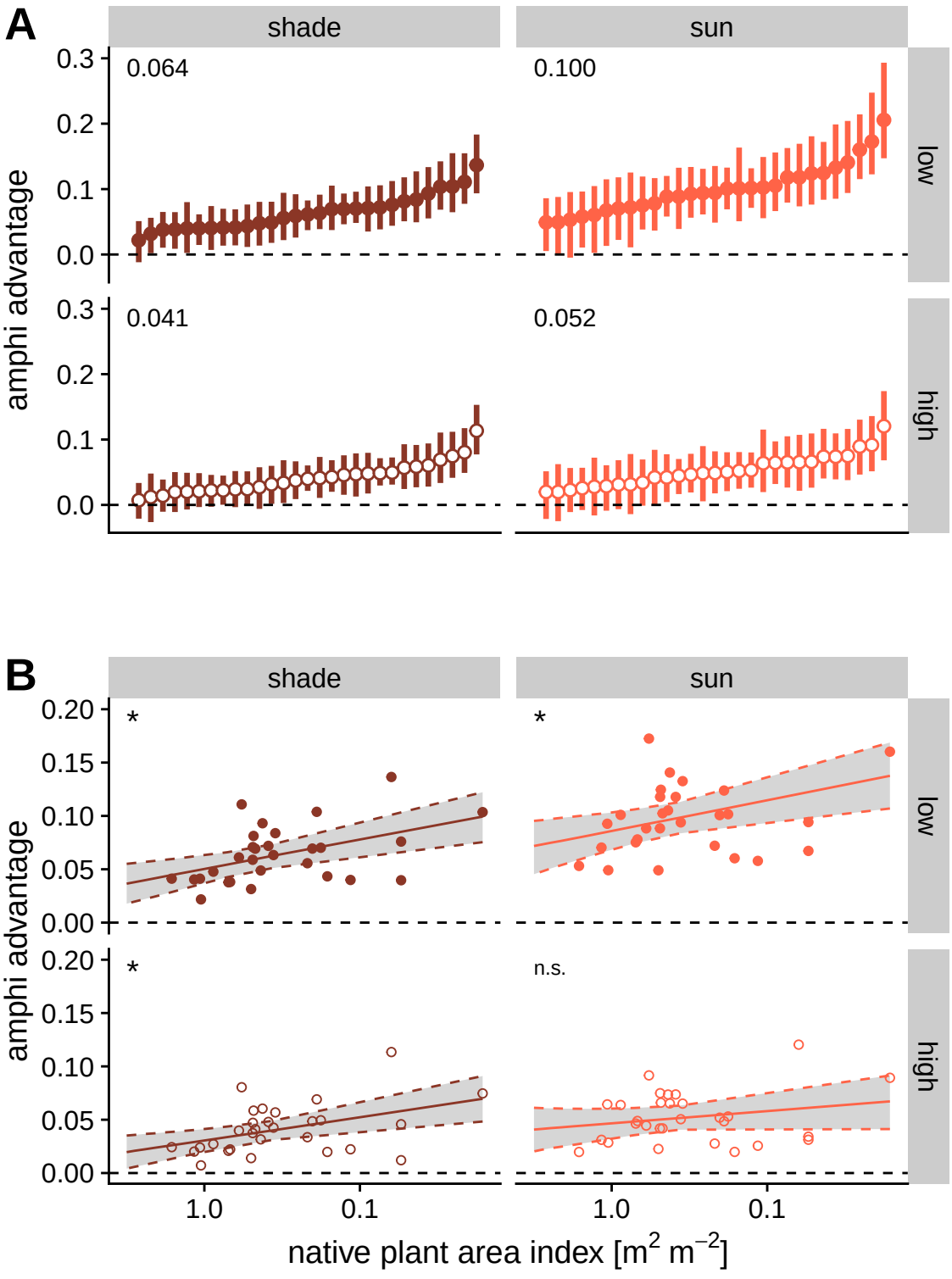

Figure 2: Caption on following page.

Figure 2: **Amphistomy advantage (**AA**) in greater wild tomatoes from open habitats and is further amplified by developmental plasticity under sunny growth conditions.** AA (y-axis) is the log-response ratio of photosynthesis in an amphistomatous leaf compared to an otherwise identical pseudohypostomatous leaf. In both panels, estimates are shown for plants grown under simulated shade (brown) or sun (orange) and measured under high light intensity (PPFD $=$ 2000 µmol m^{-2} s^{-1}; open circles) and low light intensity (PPFD $= 150$ µmol m^{-2} s^{-1}; solid circles). The dashed line at zero indicates no difference in photosynthesis between amphi- and pseudohypostomatous leaves. (**A**) The points are the posterior median AA for each population, with error bars showing 95% confidence intervals. Within each facet, the populations are arranged by AA estimated in that growth and measurement condition. The average AA among populations for each treatment group is written in the top left corner. (**B**) The same estimates of AA in each combination of growth and measurement light intensity ploted against native plant area index (PAI; x-axis, log-scale). The confidence intervals were omitted for visual clarity. The median relationship between native PAI (x-axis; log-scale) and AA is shown as a solid line with the shaded region between dashed lines showing the 95% confidence ribbon. The * in the top left corner of each facet indicates the slope of the linear regression is significantly different from zero; n.s. indicates not significant.

We conclude that both developmental plasticity and adaptation to open habitats, but not acclimation, may explain the long-standing observation that amphistomatous leaves are more common in sunny habitats, at least among herbaceous plants including crop relatives. This result changes our understanding by showing high light intensity *per se* does not increase the benefit of amphistomy, but rather arise as a byproduct of anatomical and biochemical changes caused by plasticity and adaptation to higher light intensity modulate AA. To gain more precise understanding of when amphistomy is most beneficial will require further research on its leaf anataomical and biochemical basis.

The magnitude of AA we document across populations is also noteworthy, as it implies that hypostomatous leaves predominant in mesic to wet forests globally are giving up 'free' carbon that would require little to no additional water loss. The cost of hypostomy can be quantified as the difference in total g_{sw} that an amphistomatous leaf would require to achieve the same photosynthetic rate. This cost can be locally approximated on a log-ratio scale as AA/ε_g (Supporting Information), where ε_g is the elasticity of A to g_{sw}. For $\text{AA} = 0.05$, the water cost of hypostomy would be 0.5 (64.9%) at low elasticities ($\varepsilon_g = 0.1$) and 0.1 (10.5%) at high elasticities ($\varepsilon_g = 0.5$). For plants to expend this much extra water implies a large fitness cost of upper stomata in certain ecological contexts. As this is the first quantitative comparison of AA across species, estimation from a broader range of species and environments will be required to fully understand the ecological causes and consequences of stomatal distributions on leaf surfaces.

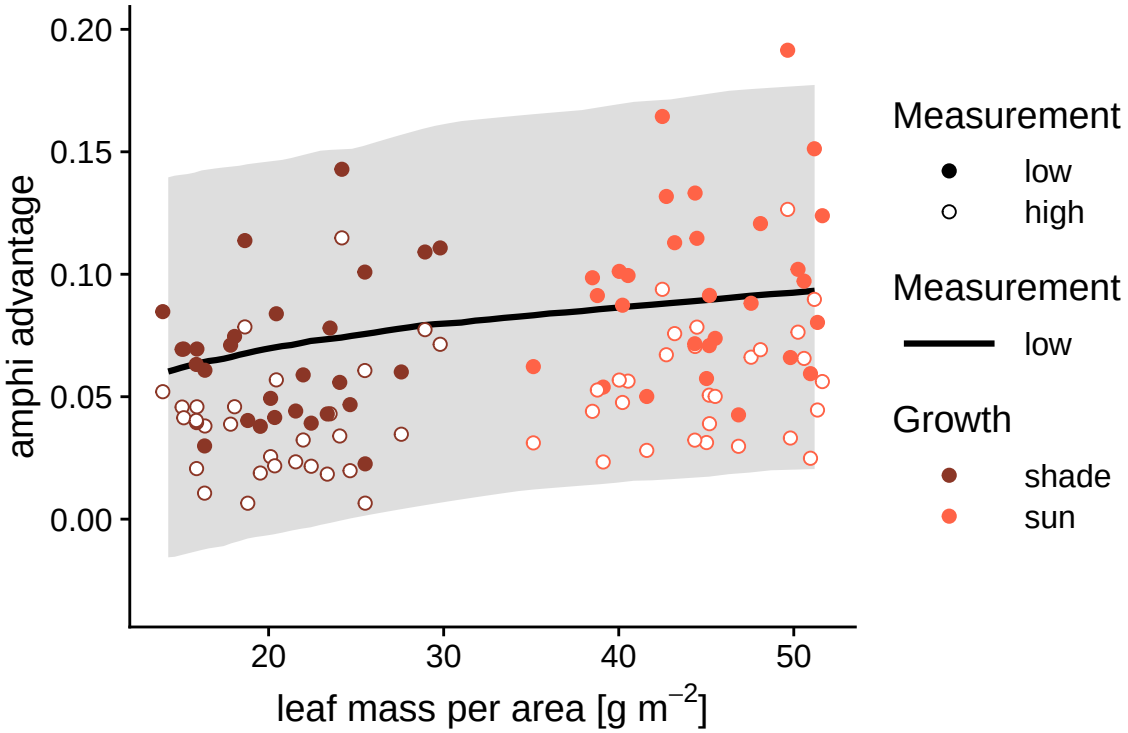

Figure 3: **Plastic changes in leaf mass per area (LMA) mediate the effect of sun- to shade-grown plants on amphistomy advantage (**AA**).** Each point is the estimated population-level LMA (x-axis) and AA (y-axis) for each population grown under high light intensity (PPFD $=$ 2000 µmol m^{-2} s^{-1}) and low light intensity (PPFD $=$ 150 µmol m^{-2} s^{-1}). The points are colored by growth light treatment. The solid line is the posterior median of the linear regression of individual-level LMA on AA_{2000} with the shaded region showing the 95% confidence ribbon; the dashed line is the same for AA_{150}. Confidence intervals for each population estimate were omitted for visual clarity.

Acknowledgements

Sam McKlin and Tom Buckley helped with protocol development. Justin Alter, Max Gatlin, Joana Kim, Jenna Matsuyama, Brandon Najarian, and Kai Yasuda contributed to data collection. Sarah Friedrich helped with graphics.

Funding:

US National Science Foundation OIA-1929167 to C.D.M.

Author contributions:

Conceptualization: C.D.M.; Methodology: C.D.M., W.S.L.; Investigation: C.D.M., W.S.L., D.W.; Visualization: C.D.M.; Funding acquisition: C.D.M.; Writing – original draft: C.D.M.; Writing – review & editing: C.D.M., W.S.L., D.W.

References

1. J. A. Raven, Selection pressures on stomatal evolution. *New Phytologist* **153**, 371–386 (2002).

2. S. A. M. McAdam, J. G. Duckett, F. C. Sussmilch, S. Pressel, K. S. Renzaglia, R. Hedrich, T. J. Brodribb, A. Merced, Stomata: The holey grail of plant evolution. *American Journal of Botany* **108**, 366–371 (2021).

3. J. W. Clark, B. J. Harris, A. J. Hetherington, N. Hurtado-Castano, R. A. Brench, S. Casson, T. A. Williams, J. E. Gray, A. M. Hetherington, The origin and evolution of stomata. *Current Biology* **32**, R539–R553 (2022).

4. A. M. Hetherington, F. I. Woodward, The role of stomata in sensing and driving environmental change. *Nature* **424**, 901–908 (2003).

5. H. J. de Boer, C. A. Price, F. Wagner□Cremer, S. C. Dekker, P. J. Franks, E. J. Veneklaas, Optimal allocation of leaf epidermal area for gas exchange. *New Phytologist* **210**, 1219–1228 (2016).

6. E. L. Harrison, L. Arce Cubas, J. E. Gray, C. Hepworth, The influence of stomatal morphology and distribution on photosynthetic gas exchange. *The Plant Journal* **101**, 768–779 (2020).

7. F. I. Woodward, Stomatal numbers are sensitive to increases in CO2 from pre-industrial levels. *Nature* **327**, 617–618 (1987).

8. T. N. Buckley, K. A. Mott, Modelling stomatal conductance in response to environmental factors: Modelling stomatal conductance. *Plant, Cell & Environment* **36**, 1691–1699 (2013).

9. M. Haworth, C. Elliott-Kingston, J. C. McElwain, Co-ordination of physiological and morphological responses of stomata to elevated [CO2] in vascular plants. *Oecologia* **171**, 71–82 (2013).

10. X. Liang, D. Wang, Q. Ye, J. Zhang, M. Liu, H. Liu, K. Yu, Y. Wang, E. Hou, B. Zhong, L. Xu, T. Lv, S. Peng, H. Lu, P. Sicard, A. Anav, D. S. Ellsworth, Stomatal responses of terrestrial plants to global change. *Nature Communications* **14**, 2188 (2023).

11. L. C. Chua, O. S. Lau, Stomatal development in the changing climate. *Development* **151**, dev202681 (2024).

12. P. L. M. Lang, J. M. Erberich, L. Lopez, C. L. Weiß, G. Amador, H. F. Fung, S. M. Latorre, J. R. Lasky, H. A. Burbano, M. Expósito-Alonso, D. C. Bergmann, Century-long timelines of herbarium genomes predict plant stomatal response to climate change. *Nature Ecology & Evolution* **8**, 1641–1653 (2024).

13. P. J. Franks, D. L. Royer, D. J. Beerling, P. K. Van de Water, D. J. Cantrill, M. M. Barbour, J. A. Berry, New constraints on atmospheric CO_2 concentration for the Phanerozoic. *Geophysical Research Letters* **41**, 4685–4694 (2014).

14. J. C. McElwain, M. Steinthorsdottir, Paleoecology, ploidy, paleoatmospheric composition, and developmental biology: A review of the multiple uses of fossil stomata. *Plant Physiology* **174**, 650–664 (2017).

15. The Cenozoic CO Proxy Integration Project (CenCOPIP) Consortium*†, B. Hönisch, D. L. Royer, D. O. Breecker, P. J. Polissar, G. J. Bowen, M. J. Henehan, Y. Cui, M. Steinthorsdottir, J. C. McElwain, M. J. Kohn, A. Pearson, S. R. Phelps, K. T. Uno, A. Ridgwell, E. Anagnostou, J. Austermann, M. P. S. Badger, R. S. Barclay, P. K. Bijl, T. B. Chalk, C. R. Scotese, E. De La Vega, R. M. DeConto, K. A. Dyez, V. Ferrini, P. J. Franks, C. F. Giulivi, M. Gutjahr, D. T. Harper, L. L. Haynes, M. Huber, K. E. Snell, B. A. Keisling, W. Konrad, T. K. Lowenstein, A. Malinverno, M. Guillermic, L. M. Mejía, J. N. Milligan, J. J. Morton, L. Nordt, R. Whiteford, A. Roth-Nebelsick, J. K. C. Rugenstein, M. F. Schaller, N. D. Sheldon, S. Sosdian, E. B. Wilkes, C. R. Witkowski, Y. G. Zhang, L. Anderson, D. J. Beerling, C. Bolton, T. E. Cerling, J. M. Cotton, J. Da, D. D. Ekart, G. L. Foster, D. R. Greenwood, E. G. Hyland, E. A. Jagniecki, J. P. Jasper, J. B. Kowalczyk, L. Kunzmann, W. M. Kürschner, C. E. Lawrence, C. H. Lear, M. A. Martínez-Botí, D. P. Maxbauer, P. Montagna, B. D. A. Naafs, J. W. B. Rae, M. Raitzsch, G. J. Retallack, S. J. Ring, O. Seki, J. Sepúlveda, A. Sinha, T. F. Tesfamichael, A. Tripati, J. Van Der Burgh, J. Yu, J. C. Zachos, L. Zhang, Toward a Cenozoic history of atmospheric CO_2. *Science* **382**, eadi5177 (2023).

16. T. A. Hofmann, W. Atkinson, M. Fan, A. J. Simkin, P. Jindal, T. Lawson, Impact of climate-driven changes in temperature on stomatal anatomy and physiology. *Philosophical Transactions of the Royal Society B: Biological Sciences* **380**, 20240244 (2025).

17. J. A. Berry, D. J. Beerling, P. J. Franks, Stomata: Key players in the earth system, past and present. *Current Opinion in Plant Biology* **13**, 232–239 (2010).

18. P. J. Franks, J. A. Berry, D. L. Lombardozzi, G. B. Bonan, Stomatal Function across Temporal and Spatial Scales: Deep-Time Trends, Land-Atmosphere Coupling and Global Models. *Plant Physiology* **174**, 583–602 (2017).

19. P. J. Grubb, "Leaf structure and function" in *The Encyclopedia of Ignorance*, R. Duncan, M. Weston-Smith, Eds. (Pergamon, Oxford, 1977)vol. 2, pp. 317–330.

20. D. F. Parkhurst, The adaptive significance of stomatal occurrence on one or both surfaces of leaves. *The Journal of Ecology* **66**, 367–383 (1978).

21. K. A. Mott, A. C. Gibson, J. W. O'Leary, The adaptive significance of amphistomatic leaves. *Plant, Cell & Environment* **5**, 455–460 (1982).

22. A. C. Gibson, *Structure-Function Relations of Warm Desert Plants* (Springer Berlin / Heidelberg, Berlin, Heidelberg, 1996; http://public.eblib.com/choice/PublicFullRecord.aspx?p=6495247).

23. W. K. Smith, T. C. Vogelmann, E. H. DeLucia, D. T. Bell, K. A. Shepherd, Leaf Form and Photosynthesis. *BioScience* **47**, 785–793 (1997).

24. R. Oguchi, Y. Onoda, I. Terashima, D. Tholen, "Leaf Anatomy and Function" in *The Leaf: A Platform for Performing Photosynthesis*, W. W. Adams III, I. Terashima, Eds. (Springer International Publishing, Cham, 2018; https://doi.org/10.1007/978-3-319-93594-2_5)*Advances in Photosynthesis and Respiration*, pp. 97–139.

25. P. L. Drake, H. J. de Boer, S. J. Schymanski, E. J. Veneklaas, Two sides to every leaf: Water and CO_2 transport in hypostomatous and amphistomatous leaves. *New Phytologist* **222**, 1179–1187 (2019).

26. P. J. Grubb, "Leaf structure and function" in *Unsolved Problems in Ecology*, A. Dobson, D. Tilman, R. D. Holt, Eds. (Princeton University Press, Princeton, 2020), pp. 124–144.

27. J. Pospíšilová, J. Solárová, Environmental and biological control of diffusive conductances of adaxial and abaxial leaf epidermes. *Photosynthetica* **14**, 90–127 (1980).

28. K. A. Mott, J. W. O'Leary, Stomatal Behavior and CO□ Exchange Characteristics in Amphistomatous Leaves. *Plant Physiology* **74**, 47–51 (1984).

29. P. B. Reich, A. W. Schoettle, R. G. Amundson, Effects of low concentrations of O3, leaf age and water stress on leaf diffusive conductance and water use efficiency in soybean. *Physiologia Plantarum* **63**, 58–64 (1985).

30. K. A. Mott, Z. G. Cardon, J. A. Berry, Asymmetric patchy stomatal closure for the two surfaces of *Xanthium strumarium* L. Leaves at low humidity. *Plant, Cell & Environment* **16**, 25–34 (1993).

31. S. Wall, S. Vialet□Chabrand, P. Davey, J. Van Rie, A. Galle, J. Cockram, T. Lawson, Stomata on the abaxial and adaxial leaf surfaces contribute differently to leaf gas exchange and photosynthesis in wheat. *New Phytologist* **235**, 1743–1756 (2022).

32. V. P. Gutschick, Photosynthesis model for C_3 leaves incorporating CO_2 transport, propagation of radiation, and biochemistry 2. Ecological and agricultural utility. *Photosynthetica* **18**, 569–595 (1984).

33. D. A. Márquez, H. Stuart□Williams, L. A. Cernusak, G. D. Farquhar, Assessing the CO_2 concentration at the surface of photosynthetic mesophyll cells. *New Phytologist* **238**, 1446–1460 (2023).

34. D. F. Parkhurst, K. A. Mott, Intercellular diffusion limits to CO_2 uptake in leaves: Studies in air and helox. *Plant Physiology* **94**, 1024–1032 (1990).

35. J. R. Foster, W. K. Smith, Influence of stomatal distribution on transpiration in low-wind environments. *Plant, Cell and Environment* **9**, 751–759 (1986).

36. C. D. Muir, Is amphistomy an adaptation to high light? Optimality models of stomatal traits along light gradients. *Integrative and Comparative Biology* **59**, 571–584 (2019).

37. J. G. Wood, The physiology of xerophytism in Australian plants: The stomatal frequencies, transpiration and osmotic pressures of sclerophyll and tomentose-succulent leaved plants. *Journal of Ecology* **22**, 69–87 (1934).

38. J. T. Howell, Concerning stomata on leaves in *a*rctostaphylos. *The Wasmann Collector* **6**, 57–65 (1945).

39. E. J. Salisbury, I. On the causes and ecological significance of stomatal frequency, with special reference to the woodland flora. *Philosophical Transactions of the Royal Society of London. Series B, Containing Papers of a Biological Character* **216**, 1–65 (1928).

40. H. J. Peat, A. H. Fitter, A comparative study of the distribution and density of stomata in the British flora. *Biological Journal of the Linnean Society* **52**, 377–393 (1994).

41. G. J. Jordan, R. J. Carpenter, T. J. Brodribb, Using fossil leaves as evidence for open vegetation. *Palaeogeography, Palaeoclimatology, Palaeoecology* **395**, 168–175 (2014).

42. S. F. Bucher, K. Auerswald, C. Grün-Wenzel, S. I. Higgins, J. Garcia Jorge, C. Römermann, Stomatal traits relate to habitat preferences of herbaceous species in a temperate climate. *Flora* **229**, 107–115 (2017).

43. C. D. Muir, Light and growth form interact to shape stomatal ratio among British angiosperms. *New Phytologist* **218**, 242–252 (2018).

44. G. Triplett, A. S. David, Stomatal distribution and post□fire recovery: Intra□ and interspecific variation in plants of the pyrogenic Florida scrub. *American Journal of Botany*, e70050 (2025).

45. O. B. Lyshede, Comparative and functional leaf anatomy of selected Alstroemeriaceae of mainly Chilean origin. *Botanical Journal of the Linnean Society* **140**, 261–272 (2002).

46. G. Triplett, T. N. Buckley, C. D. Muir, Amphistomy increases leaf photosynthesis more in coastal than montane plants of Hawaiian ʻilima (*Sida fallax*). *American Journal of Botany* **111**, e16284 (2024).

47. H. Poorter, Ü. Niinemets, N. Ntagkas, A. Siebenkäs, M. Mäenpää, S. Matsubara, T. L. Pons, A meta□analysis of plant responses to light intensity for 70 traits ranging from molecules to whole plant performance. *New Phytologist* **223**, 1073–1105 (2019).

48. T. J. Givnish, R. A. Montgomery, Common-garden studies on adaptive radiation of photosynthetic physiology among Hawaiian lobeliads. *Proceedings of the Royal Society B: Biological Sciences* **281**, 20132944–20132944 (2014).

49. B. M. J. Engelbrecht, H. M. Herz, Evaluation of different methods to estimate understorey light conditions in tropical forests. *Journal of Tropical Ecology* **17**, 207–224 (2001).

50. I. E. Peralta, D. M. Spooner, S. Knapp, Taxonomy of wild tomatoes and their relatives (*solanum* sect. *Lycopersicoides*, sect. *Juglandifolia*, sect. *Lycopersicon*; Solanaceae). **84** (2008).

51. P. Burns, C. R. Hakkenberg, S. J. Goetz, Multi-resolution gridded maps of vegetation structure from GEDI. *Scientific Data* **11**, 881 (2024).

52. G. P. John, C. Scoffoni, T. N. Buckley, R. Villar, H. Poorter, L. Sack, The anatomical and compositional basis of leaf mass per area. *Ecology Letters* **20**, 412–425 (2017).

53. H. G. Jones, R. O. Slatyer, Effects of Intercellular Resistances on Estimates of the Intracellular Resistance to Co2 Uptake by Plant Leaves. *Australian Journal of Biological Sciences* **25**, 443 (1972).

54. P.-G. Schoch, C. Zinsou, M. Sibi, Dependence of the stomatal index on environmental factors during stomatal differentiation in leaves of *Vigna sinensis* L.: 1. Effect of light intensity. *Journal of Experimental Botany* **31**, 1211–1216 (1980).

55. L. Sack, T. N. Buckley, The developmental basis of stomatal density and flux. *Plant Physiology* **171**, 2358–2363 (2016).

56. K. A. Mott, O. Michaelson, Amphistomy as an adaptation to high light intensity in *Ambrosia cordifolia* (Compositae). *American Journal of Botany* **78**, 76–79 (1991).

57. J. Schindelin, I. Arganda-Carreras, E. Frise, V. Kaynig, M. Longair, T. Pietzsch, S. Preibisch, C. Rueden, S. Saalfeld, B. Schmid, J.-Y. Tinevez, D. J. White, V. Hartenstein, K. Eliceiri, P. Tomancak, A. Cardona, Fiji: An open-source platform for biological-image analysis. *Nature Methods* **9**, 676–682 (2012).

58. J. L. Monteith, M. H. Unsworth, *Principles of Environmental Physics: Plants, Animals, and the Atmosphere* (Elsevier/Academic Press, Amsterdam ; Boston, 4th ed., 2013).

59. Stan Development Team, *Stan Modeling Language Users Guide and Reference Manual* (2025; https://mc-stan.org).

60. P.-C. Bürkner, **Brms** : An *r* Package for Bayesian Multilevel Models Using *stan*. *Journal of Statistical Software* **80** (2017).

61. J. Gabry, R. Češnovar, A. Johnson, S. Bronder, *Cmdstanr: R Interface to 'CmdStan'* (2025; https://mc-stan.org/cmdstanr, https://discourse.mc-stan.org).

62. R Core Team, *R: A Language and Environment for Statistical Computing* (R Foundation for Statistical Computing, Vienna, Austria, 2025; http://www.R-project.org/).

63. A. Gelman, D. B. Rubin, Inference from iterative simulation using multiple sequences. *Statistical Science* **7**, 457–472 (1992).

64. J. B. Pease, D. C. Haak, M. W. Hahn, L. C. Moyle, Phylogenomics reveals three sources of adaptive variation during a rapid radiation. *PLOS Biology* **14**, e1002379 (2016).

65. A. Vehtari, A. Gelman, J. Gabry, Practical Bayesian model evaluation using leave-one-out cross-validation and WAIC. *Statistics and Computing* **27**, 1413–1432 (2017).

Supplementary Materials

Materials and Methods

Populations

We compared AA among 29 ecologically diverse populations of wild tomato, including representatives of all described species of *Solanum* sect. *Lycopersicon* and sect. *Lycopersicoides* (*50*) and the cultivated tomato *S. lycopersicum* var. *lycopersicum* (Table S1). Due to constraints on growth space and time, we spread out measurements over 61.1 weeks from August 29, 2022 to October 31, 2023. Replicates within population were evenly spread out over this period to prevent confounding of temporal variation in growth conditions with accession. [anything else to say here? maybe explain population selection and phylogeny?]

Table S1: Accession information of *Solanum* populations used in this study. The species name, accession number, collection latitude, longitude, elevation, and plant area index (PAI) from the Global Ecosystem Dynamics Investigation (see 'Climate data'). TGRC: Tomato Genetics Resource Center.

Species	TGRC accession	Latitude	Longitude	Elevation (mas)	PAI ($m^2\ m^{-2}$)
S. arcanum	LA2172	-6.008	-78.858	662	0.70
S. cheesmaniae	LA0429	-0.644	-90.329	800	0.60
S. cheesmaniae	LA3124	-0.804	-90.042	1	0.36
S. chilense	LA1782	-15.267	-74.633	1000	0.35
S. chilense	LA4117A	-22.907	-67.941	3540	0.22
S. chmielewskii	LA1028	-13.883	-73.017	3000	0.43
S. chmielewskii	LA1316	-13.400	-73.906	2920	1.07
S. corneliomulleri	LA0107	-13.117	-76.383	60	0.02
S. corneliomulleri	LA0444	-13.433	-76.133	100	0.49
S. galapagense	LA0436	-0.953	-90.978	40	0.20
S. galapagense	LA1044	-0.284	-90.548	0	0.18
S. habrochaites	LA0407	-2.181	-79.884	70	0.47
S. habrochaites	LA1777	-9.550	-77.700	3216	0.42
S. huaylasense	LA1358	-9.533	-77.967	750	0.58
S. huaylasense	LA1360	-9.546	-77.929	1490	0.48
S. huaylasense	LA1364	-10.133	-77.383	2920	0.88
S. lycopersicoides	LA2951	-19.317	-69.450	2200	0.49
S. lycopersicoides	LA4126	-19.287	-69.396	3120	0.39
S. neorickii	LA1322	-13.483	-72.442	2380	0.68
S. neorickii	LA2133	-3.400	-79.183	1980	1.05

(continued)

Species	TGRC accession	Latitude	Longitude	Elevation (mas)	PAI ($m^2\ m^{-2}$)
S. pennellii	LA0716	-16.225	-73.617	50	0.19
S. pennellii	LA0750	-14.775	-75.034	550	0.05
S. pennellii	LA3778	-14.775	-75.034	616	0.05
S. peruvianum	LA2744	-18.550	-70.150	400	0.16
S. peruvianum	LA2964	-18.028	-70.835	75	1.16
S. pimpinellifolium	LA1269	-11.483	-77.075	400	0.50
S. pimpinellifolium	LA1589	-8.433	-78.817	30	0.11
S. pimpinellifolium	LA2933	-1.442	-80.562	375	1.62
S. sitiens	LA4116	-22.159	-68.782	2960	0.06

Plant growth conditions

In all growth spaces, we recorded PPFD using full spectrum quantum sensors (SQ-500-SS, Apogee Instruments, Logan, Utah, USA); we recorded temperature, RH, and [CO_2] using an EE894 sensor (E+E Elektronik, Engerwitzdorf, Austria) protected by a radiation shield. All environmental measurements were taken every 10 minutes from the middle of plants racks at approximately the same height as the leaves we measured. We measured leaf temperature of focal leaves prior to measurement using an infrared radiometer (SI-111-SS, Apogee Instruments, Logan, Utah, USA).

Germination and seedling stage

Seeds provided by the Tomato Genetics Resource Center germinated on moist paper in plastic boxes after soaking for 30-60 minutes in a 50% (volume per volume) solution of household bleach and water, followed by a thorough rinse. We transferred seedlings to cell-pack flats containing Pro-Mix BX potting mix (Premier Tech, Rivière-du-Loup, Quebec, Canada) once cotyledons fully emerged, typically within 1-2 weeks of sowing. We grew seeds and seedlings for both sun and shade treatments under the same environmental conditions (12:12 h, 24.3:21.7 °C, 49.6:58.4 RH day:night cycle). LED light provided PPFD $= 267\ \mu mol\ m^{-2}\ s^{-1}$ (Fluence RAZRx, Austin, Texas, USA).

Light treatments

Seedlings were randomly assigned in alternating order within population to the sun or shade treatment during transplanting. After seedlings established in cell-pack flats for $\approx$ 2 weeks, we transplanted them to 3.78 L plastic pots containing 60% Pro-Mix BX potting mix, 20% coral sand (Pro-Pak, Honolulu, Hawai‘i, USA), and 20% cinders (Niu Nursery, Honolulu, Hawai‘i, USA). Percentage composition is on a volume basis. The soil mixture contained slow release NPK fertilizer following manufacturer instructions (Osmocote Smart-Release Plant Food Flower & Vegetable, The Scotts Company, Marysville, Ohio, USA). We determined pot field capacity one week after transplanting using a scale

(Ohaus V12P15 Valor 1000, Parsippany, New Jersey, USA) and watered to field capacity three times per week to prevent drought stress.

We assigned sun and shade treatment to lower and upper racks of a $1.22\,\mathrm{m} \times 2.44\,\mathrm{m}$ shelving unit in a climate-controlled growth room. We assigned the sun treatment to the lower rack to limit diffuse light from reaching the shade treatment. The average daytime PPFD was $761\,\mu\mathrm{mol\,m^{-2}\,s^{-1}}$ and $115\,\mu\mathrm{mol\,m^{-2}\,s^{-1}}$ for sun and shade treatments, respectively. To isolate the effect of light intensity from quality, we used the same LED model with the the same spectrum (Fluence SPYDR 2i, Austin, Texas, USAS), but dimmed the lights in the shade treatment. To maintain homogeneous environmental conditions other than light, we mixed air within the growth room using an air circulator (Vornado 693DC, Andover, Kansas, USA) and within racks using a miniature oscillating air circulator (Vornado Atom 1, Andover, Kansas, USA). Despite these efforts, the air in the sun treatment was on average $2.56\,^{\circ}\mathrm{C}$ warmer and the average RH was consequently 5.75% lower. However, because of evaporative cooling, the leaves in the sun treatment were only $0.886\,^{\circ}\mathrm{C}$ on average ($n = 699$ leaves).

Leaf trait measurements

We selected a fully expanded, unshaded leaf at least six leaves above the cotyledons during early vegetative growth. This typically meant that plants had grown in light treatments for ≈ 4 weeks, ensuring they had time to sense and respond developmentally to the light intensity of the treatment rather than the seedling conditions (*54*). Shade plants grew slower than sun plants, hence leaves at the same developmental stage were measured on chronologically older plants in the shade treatment. In some sun plants, we had to use leaves higher on the stem because short internodes made lower leaves inaccessible with the gas exchange equipment. We measured terminal leaflets in 82.6% of cases, but used the lateral leaflet closest to the terminal leaflet when it was damaged or difficult to clamp into the gas exchange chamber. When a leaflet was damaged during gas exchange measurements, we collected anatomical data from the nearest leaflet on the same leaf (1.58% of leaves).

Amphistomy advantage

We estimated 'amphistomy advantage' (AA) *sensu* (*20*), but with modifications previously described in (*46*). AA is calculated as the log-response ratio of A compared at the same total g_{sw}:

$$\mathrm{AA} = \log(A_{\mathrm{amphi}}/A_{\mathrm{hypo}})$$

We measured the photosynthetic rate of an untreated amphistomatous leaf (A_{amphi}) over a range of g_{sw} values. We refer to this as an A–g_{sw} curve. We compared the A–g_{sw} curve of the untreated leaf to the photosynthetic rate of pseudohypostomatous leaf (A_{hypo}), which is the same leaf but with gas exchange through the upper surface blocked by a neutral density plastic (propafilm).

We measured A–g_{sw} curves using a portable infrared gas analyzer (LI-6800PF, LI-COR Biosciences, Lincoln, Nebraska, USA). Light-acclimated plants were placed under LEDs dimmed to match their light

treatment during gas exchange measurements. We estimated the photosynthetic rate (A) and stomatal conductance to CO_2 (g_{sw}) at ambient CO_2 ($C_a = 415\,\mu mol\,mol^{-1}$) and $T_{leaf} = 25.0\,°C$. The irradiance of the light source in the pseudohypo leaf was higher because the propafilm reduces transmission. To compensate for reduced transmission, we increased incident PPFD for pseudohypo leaves by a factor 1/0.91, the inverse of the measured transmissivity of the propafilm. We also set the stomatal conductance ratio, for purposes of calculating boundary layer conductance, to 0 for pseudohypo leaves following manufacturer directions.

We collected four A–g_{sw} curves per leaf, an amphi (untreated) curve and a pseudohypo (treated) curve at high light-intensity (PPFD $= 2000\,\mu mol\,m^{-2}\,s^{-1}$; 97.8:2.24 red:blue) and low light-intensity (PPFD $= 150\,\mu mol\,m^{-2}\,s^{-1}$; 87.0:13.0 red:blue). We always measured high light-intensity curves first because photosynthetic downregulation is faster than upregulation in these species. To control for order effects, we alternated between starting with amphi or pseudohypo leaf measurements. Unlike (*46*), preliminary experiments with *Solanum* indicated a strong order effect in that A declined in the second curve. Therefore, we made measurements over two days. On the first day, we measured high and low light-intensity curves for either amphi or pseudohypo leaves; on the second day, we measured high and low light-intensity curves on the other leaf type.

In all cases, we acclimated the focal leaf to high light (PPFD $= 2000\,\mu mol\,m^{-2}\,s^{-1}$) and high relative humidity (RH $= 70\%$) until A and g_{sw} reach their maximum. After that, we decreased RH to $\approx 10\%$ to induce rapid stomatal closure without biochemical downregulation. Hence, A_{amphi} and A_{hypo} were both measured at low chamber humidity after the leaf had acclimated to high humidity. All other environmental conditions in the leaf chamber remained the same. We logged data until g_{sw} reached its nadir. We then acclimated the leaf to low light (PPFD $= 150\,\mu mol\,m^{-2}\,s^{-1}$) and RH $= 70\%$ before inducing stomatal closure with low RH and logging data as described above.

Light-saturated photosynthetic rate

In 91.3% of plants, we measured the maximum photosynthetic rate (A_{max}) on the same leaflets as A–g_{sw} curves. However, when a leaflet was damaged during A–g_{sw} curves, we used the next closest leaflet for A_{max}. Leaves acclimated to high light-intensity (PPFD $= 2000\,\mu mol\,m^{-2}\,s^{-1}$), ambient CO_2 ($C_a = 415\,\mu mol\,mol^{-1}$), RH $= 50\%$, and $T_{leaf} = 25\,°C$. After A and g_{sw} stabilized, we measured A at $2000\,\mu mol\,m^{-2}\,s^{-1}$.

Stomatal anatomy

We estimated the stomatal density and size on ab- and adaxial leaf surfaces from all leaves, using guard cell length as a proxy for stomatal size since it is proportional to maximum conductance (*55*). We made surface impressions of leaf lamina from the same area used for gas exchange measurements using a-silicone impression material (Zhermack elite HD+, light body, fast set, Rovigo, Italy). We applied clear nail polish to make positive replicas of the impression. After nail polish dried, we mounted replicas on a microscope slide using transparent tape (*56*). We digitized a portion of each leaf surface replica using a brightfield microscope (Leica DM2000, Wetzlar, Germany). We counted and measured guard

cell length on all stomata using the FIJI implementation of ImageJ2 version 2.3.0 (*57*), then divided the count by the visible leaf area ($0.890\ \text{mm}^2$) to estimate stomatal density. For each surface we calculated the anatomical maximum stomatal conductance (g_{max}) at a reference leaf temperature of 25 °C following (*55*) as:

$$g_{\text{max}} = bmD_{\text{S}}A_{\text{S}}.$$

The biophysical and morphological constants b and m are:

$$b = \frac{D_{\text{wv}}}{v}, \text{ and}$$

$$m = \frac{\pi c^2}{j^{0.5}(4hj + \pi c)},$$

where D_{wv} is the diffusion coefficient of water vapor in air and v is by the kinematic viscosity of dry air. We assumed $D_{\text{wv}} = 2.49 \times 10^{-5}\ \text{m}^2\ \text{s}^{-1}$ and $v = 2.24 \times 10^{-2}\ \text{m}^3\ \text{mol}^{-1}$ (*58*). For kidney-shaped guard cells like those in wild tomatoes, $c = h = j = 0.5$. The $g_{\text{max,ratio}}$ is the g_{max} of the adaxial surface divided by the sum total g_{max} of both surfaces.

Leaf mass per area

Leaf mass per area (LMA) is the dry mass divided by the leaflet area. We scanned fresh leaflets on a flat bed scanner (Epson V600, Los Alamitos, California. USA) and measured leaflet area from digital images using the FIJI implementation of ImageJ2 version 2.3.0 (*57*). We dried leaves for 72 hours at 74 °C in a food dehydrator (Cosori CP267-FD, Vesync Co., Anaheim, California, USA) and weighed using a benchtop analytical balance (Ohaus PR64 Analytical Balance, Parsippany, New Jersey, USA). In 10.5% of leaves we measured LMA on the adjacent leaflet because the focal leaflet was damaged or wilted while making surface impressions and we could not reliably estimate area. LMA data are missing from 2.97% of individuals because the area or mass was not recorded at all or recorded incorrectly.

Cleaning A–g_{sw} curves

The raw data set consisted of 2,370 A–g_{sw} curves with an average of 63.2 points per curve. Manual curation of a data set this size in a principled, consistent manner is not feasible. Therefore, we automated data cleaning using custom *R* scripts. Cleaning is divided into six sequential steps (Table S2).

Table S2: Six sequential steps for cleaning A–g_{sw} curves. The rationale and procedure for each step are described in the text. The rightmost columns summarize the number of curves and mean number of points per curve remaining after each step. For reference, there are four possible A–g_{sw} curves per replicate: all combinations of leaf type (amphi or pseudohypo) and light intensity (high or low).

Step: description	Number of curves	Number of points per curve
1. remove unreliable and unusable data points	2,361	63.0
2. remove hysteretic portion of A–g_{sw} curves at low g_{sw}	2,360	59.2
3. remove outliers within each A–g_{sw} curve	2,360	58.7
4. remove replicates with no overlap between amphi and pseudohypo A–g_{sw} curves	2,268	58.4
5. thin redundant data points within each A–g_{sw} curve	2,268	28.1
6. trim extreme AA values	2,214	28.1

Remove unreliable and unusable data points

Rationale: Unreliable data points consisted of those where chamber [CO_2] was unstable and therefore measurements are not biologically meaningful. Unusable data points were those where $A < 0$ because the logarithm of a negative number is undefined.

Procedure: We retained data points where $410 < C_a < 420\,\mu mol\,mol^{-1}$ and $A > 0$.

Remove hysteretic portion of A–g_{sw} curves at low g_{sw}

Rationale: In most A–g_{sw} curves, we observed a hysteretic response at low g_{sw}. After g_{sw} and A declined simultaneously, A increased slightly as g_{sw} continued to decline or stabilize, indicating some leaf acclimation to low RH. We removed this portion of the curve to focus curve-fitting on the primary domain where A increases monotonically with g_{sw}.

Procedure: For each curve, we removed data points after g_{sw} had reached its minimum unless there were fewer than 10 data points remaining.

Remove outliers within each A–g_{sw} curve

Rationale: Individual outliers within A–g_{sw} curves, usually caused by transitory changes in chamber conditions, exert undue leverage on parameter estimates and cause bias and/or low precision in parameter estimates.

Procedure: We fit provisional quadratic regressions for each curve using ordinary least squares with the `lm()` function in *R*. We sequentially removed data points with an absolute external studentized residual > 3 until none remained.

Thin redundant data points within each A–g_{sw} curve

Rationale: Data points closely spaced along the A–g_{sw} curve provide redundant information and may be highly correlated (i.e. pseudoreplication). This occurred because data was logged at a constant temporal interval, but the rate at which g_{sw} declined was not constant. Thinning reduces parameter estimation bias toward densely sampled regions of the curve which may not be the most biologically informative.

Procedure: We retained the maxima and minima g_{sw} for each curve and thinned all but one point per thinning interval of $0.05\ \log(\text{mol}\,\text{m}^{-2}\,\text{s}^{-1})$, retaining the point nearest the midpoint of the interval.

Remove replicates with no overlap between amphi and pseudohypo A–g_{sw} curves

Rationale: We could not estimate AA for replicates where amphi and pseudohypo A–g_{sw} curves did not overlap.

Procedure: We removed replicates where the range of g_{sw} values for amphi and pseudohypo A–g_{sw} curves did not overlap.

Trim extreme AA values

Rationale: Extreme AA values were likely due to measurement error or leaf damage. Since amphi and pseudohypo A–g_{sw} curves are measured on consecutive days, a poor calibration or a damaged leaf could cause a large difference in A between days, which would appear as an extreme AA value.

Procedure: We provisionally estimated AA for each replicate by integrating over the range of g_{sw} values where amphi and pseudohypo A–g_{sw} curves overlap. In this procedure, curve parameters were provisionally estimated using ordinary least squares with the `lm()` function in *R*. We then used point estimates of AA for each replicate as the response variable in a linear model with light treatment, light intensity, population, and all interactions as explanatory variables. This model was also fit using ordinary least squares with the `lm()` function in *R*. We classified extreme AA values as those with an absolute internal studentized residual > 3. Because these values likely indicate significant measurement error or leaf damage, we removed A–g_{sw} curves at both light intensities if either was classified as extreme.

Bayesian data analysis with *Stan*

Our analysis pipeline consisted of four main steps:

1. Estimate A–g_{sw} curve parameters for each leaf
2. Estimate AA for both measurement light intensities using A–g_{sw} curve parameters
3. Estimate the effects of light intensity, light treatment, and population on AA (acclimation and plasticity hypotheses)
4. Estimate the effects of native light habitat on population-level AA (constitutive hypothesis)

All models were using a Bayesian model with HMC sampling in the probabilistic programming language *Stan* (*59*) using the *R* package **brms** version 2.22.0 (*60*). We used *CmdStan* version 2.36.0 and **cmdstanr** version 0.9.0 (*61*) to interface with *R* version 4.5.1 (*62*). We sampled the posterior distribution from a single chain with a minimum of 1000 iterations after 1000 warmup iterations. If necessary, we refit models with more iterations to decrease the Gelman-Rubin convergence statistic ($\hat{R}$) (*63*) to less than 1.01 and the bulk effective sample size (ESS) to greater than 400 for all model parameters, and there were fewer than 10 divergent transitions.

A–g_{sw} curve parameters

We modeled $\log(A)$ as a quadratic function of $\log(g_{sw})$ for each leaf, measured at low and high light intensity, in both amphistomatous (untreated) and pseudohypostomatous (propafilm treatment) states.

AA for each light intensity within leaf using A–g_{sw} curve parameters

We estimated AA for each light intensity by integrating the difference in $\log(A)$ between the amphi and pseudohypo A–g_{sw} curves over the range of g_{sw} values where the curves overlap (from $\min(\log(g_{sw}))$ to $\max(\log(g_{sw}))$).

$$\widehat{\text{AA}} = \int_{\min(\log(g_{sw}))}^{\max(\log(g_{sw}))} \log\left(\frac{\hat{A}_{\text{amphi}}(x;\theta_{\text{amphi}})}{\hat{A}_{\text{hypo}}(x;\theta_{\text{hypo}})}\right) dx$$

where θ_{amphi} and θ_{hypo} are the quadratic parameters of the amphi and pseudohypo A–g_{sw} curves, respectively (Figure S1). We calculated $\widehat{\text{AA}}$ from each draw of the posterior for the paired amphi and pseudohypo A–g_{sw} curves to obtain the posterior distribution of $\widehat{\text{AA}}$ for each leaf at each light intensity. We then summarized the posterior distribution of $\widehat{\text{AA}}$ for each leaf at each light intensity by the posterior median and standard deviation, which became our point estimate of, and uncertainty in, $\widehat{\text{AA}}$ for the phylogenetic mixed effects model described below.

Phylogenetic mixed effects models

We fit Bayesian mixed effects models with phylogenetically structured random effects to test predictions of competing hypotheses about why amphistomy advantage (AA) might be greater for leaves in sunny, open habitats. We fit all models combinations of measurement light intensity, growth light intensity, and their interaction as both fixed effects and random effects among populations. In other words, we test whether there were main effects of light intensity treatments and/or whether populations varied in their response to light intensity treatments. In all models, we included population as a phylogenetically structured random effect. We accounted for uncertainty in $\widehat{\text{AA}}$ using the standard deviation of the posterior distribution of each $\widehat{\text{AA}}$ estimate (Section). We crossed fixed and random effect structures with fixed effects of measurement light intensity and/or growth light intensity on the distributional parameter, σ, the residual variance in AA. We used a robust regression approach by assuming t-distributed residuals, which makes estimates less susceptible to extreme values. In total, we

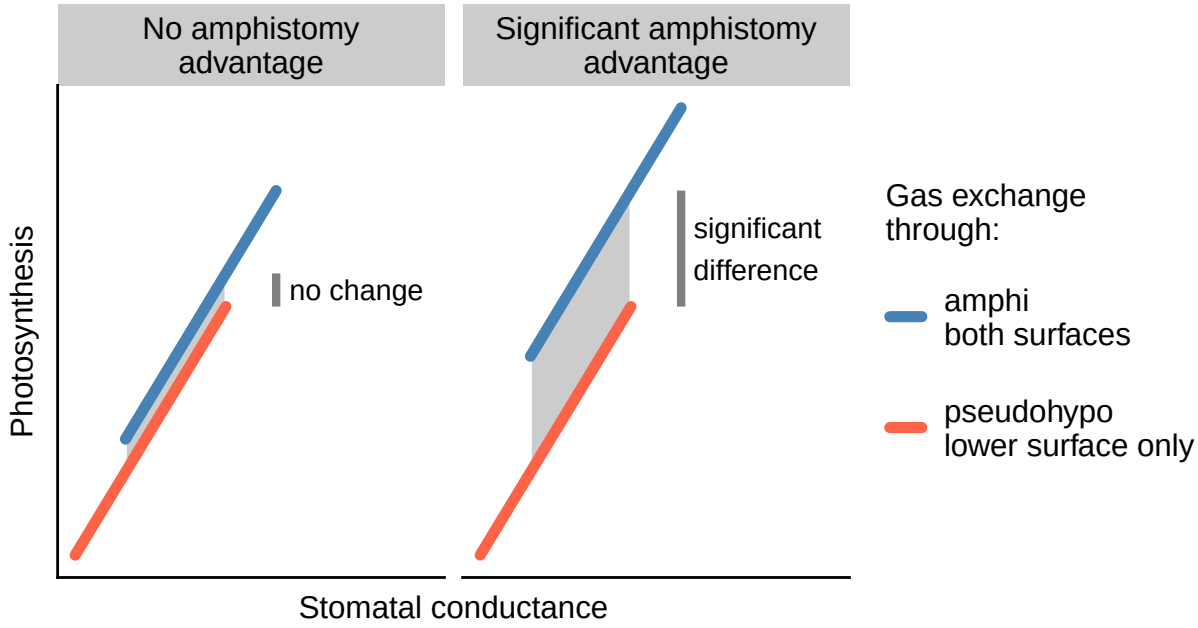

Figure S1: Example amphistomy advantage (AA) calculation from A–g_{sw} curves in an amphistomatous leaf with gas exchange through both surfaces (blue) and the same leaf with gas exchange blocked on the upper surface only (orange). We integrate over the gray region between the curves to estimate AA. The AA is low (left facet) when the photosynthetic rate of an amphistomatous leaf is similar to a pseudohypostomatous leaf at the same total stomatal conductance (x-axes); large AA (right facet) is indicated when an amphistomatous leaf has a higher photosynthetic rate than a pseudohypostomatous leaf.

fit 100 models, each with a different combination of fixed, random, and distributional effects. We used the RAxML whole-transcriptome concatenated phylogeny based on 2,745 100-kb genomic windows from (*64*). Two of our populations were not in this tree. We used accession LA1044 in place of LA3909, two populations of *S. galapagnse*; LA0750 was added as sister to LA0716, two closely related populations of *S. pennellii*. The node separating LA0750 from LA0716 was placed half-way between the next deepest node. We used the leave-one-out cross-validation information criterion (LOOIC) to compare the fit of models (Table S6) using the *R* package **loo** version 2.8.0 (*65*) to calculate LOOIC values. We selected the model with the lowest LOOIC value (Table S6) to generate posterior predictions for hypothesis testing. Parameter estimates from the selected model are shown in Table S4.

To test whether LMA mediated the relationship between growth light intensity and AA, we repeated a similar model comparison procedure but included log LMA as an additional fixed effect in the model, as well its interaction with measurement and growth light intensity. The model included a direct effect of growth light intensity on log LMA and random phylogeneticlly structured effects of population on log LMA and effects of sun treatment on log LMA. This enabled us to disentangle whether log LMA effects AA directly or indirectly because both traits respond to growth light intensity. We integrated over missing LMA data using the `mi()` function in **brms**. Because the evidence strong supported including effects of growth and measurement light intensity on the residual variance in AA, we included these in terms in all models. In total, we fit 75 models, each with a different combination of fixed and random effect structures. We selected the model with the lowest LOOIC value (Table S7) to generate posterior predictions for hypothesis testing. Note that LOOIC was calculated only from pointwise likelihood values of the submodel estimating effects of light intensity, light treatments, and population on AA. Parameter estimates from the selected model are shown in Table S5.

Posterior predictions

The acclimation, plasticity, and constitutive hypotheses make different predictions about the relationship between AA and light intensity, light treatment, and native PPFD among populations. Since these hypotheses are not mutually exclusive, we describe how we assessed support for one, two, or all three hypotheses simultaneously in Table S3. In general, the acclimation hypothesis was supported if AA was greater at high light intensity than low light intensity. The plastic hypothesis was supported if AA was greater in sun leaves than shade leaves. The constitutive hypothesis was supported if population-level AA increased with native PPFD. In interactive models, we only consider positively reinforcing interactions between high light intensity, sun leaves, and native PPFD because these are the only interactions which could explain why amphistomatous leaves are advantageous in high light habitats.

From the posterior of the selected model (Section), we predicted the posterior distribution of the expected AA for each population at each measurement light intensity and growth light intensity. If the 95% confidence intervals for AA did not overlap zero, we considered AA to be significantly different from zero. We also calculated posterior distribution for the average AA among populations in each condition. We tested a linear effect of native light habitat on population-level AA in each treatment condition, integrating over the entire posterior distribution. We calculated the posterior distribution of

the slope. If the 95% confidence interval for the slope did not overlap zero, we considered the slope to be significant.

Table S3: Predictions of competing hypotheses about the relationship between AA and light intensity, light treatment, and native plant area index (PAI) among populations. The middle column lists specific directional predictions about parameter values. The rightmost column describes the predictions in words and explains how population-level AA is calculated in the relevant model.

Hypothesis	**Prediction(s)**	**Description**
Acclimation	$AA_{2000} > 0$	AA at high light intensity is greater than that at low light intensity
Plasticity	$AA_{sun} > 0$	AA in sun leaves is greater than that in shade leaves
Constitutive	$\beta_{PAI,AA} > 0$	Population-level AA (AA_{pop}) decreases with native PAI $AA_{pop} = \beta_{AA,0} + \vec{\beta}_{AA,pop}$
Acclimation × Plasticity	$AA_{2000,sun} > 0$	AA is highest at high light intensity in sun leaves
Acclimation × Constitutive	$AA_{2000} > 0$	AA at high light intensity is greater than that at low light intensity
	$\beta_{PAI,AA} > 0$	Population-level AA at high light intensity ($AA_{pop,2000}$) decreases with native PAI $AA_{pop,2000} = \beta_{AA,0} + \vec{\beta}_{AA,pop} + \vec{\beta}_{AA,2000,pop}$
Plasticity × Constitutive	$AA_{sun} > 0$	AA in sun leaves is greater than that in shade leaves
	$\beta_{PAI,AA} > 0$	Population-level AA in sun leaves ($AA_{pop,sun}$) decreases with native PAI $AA_{pop,sun} = \beta_{AA,0} + \vec{\beta}_{AA,pop} + \vec{\beta}_{AA,sun,pop}$
Acclimation × Plasticity × Constitutive	$AA_{2000,sun} > 0$	AA is highest at high light intensity in sun leaves
	$\beta_{PAI,AA} > 0$	Population-level AA at high light intensity in sun leaves ($AA_{pop,2000,sun}$) decreases with native PAI $AA_{pop,2000,sun} =$ $\beta_{AA,0} + \vec{\beta}_{AA,pop} + \vec{\beta}_{AA,2000,pop} + \vec{\beta}_{AA,sun,pop}$

Estimating the water cost of hypostomy

Amphistomy advantage implies that hypostomatous leaves would need to lose more water by having higher g_{sw} to achieve the same photosynthetic rate. We estimated this cost of hypostomy approximately. For simplicity, we focus on a sufficiently small region of the A–g_{sw} curve such that we can approximate the relationship between g_{sw} and A as log-log linear. We also assume that slope is same in both amphistomatous and hypostomatous leaves, which was often approximately the case in our experiment (Figure S3). With these assumptions, the approximate water cost of hypostomy can be derived from the equations:

$$\log(A_{\text{amphi}}) = \beta_{\text{amphi}} + \varepsilon_g \log(g_{\text{sw}}), \text{ and}$$
$$\log(A_{\text{hypo}}) = \beta_{\text{hypo}} + \varepsilon_g \log(g_{\text{sw}}).$$

Solving for the difference in $\log g_{sw}$ at a given $\log A_{hypo}$ is:

$$\log(g_{\text{sw,amphi}}) - \log(g_{\text{sw,hypo}}) = \frac{\beta_{\text{amphi}} - \beta_{\text{hypo}}}{\varepsilon_g}.$$

Noting that because the curves are parallel, $\text{AA} = \log(A_{\text{amphi}}/A_{\text{hypo}}) = \beta_{\text{amphi}} - \beta_{\text{hypo}}$, this reveals that the negative log-ratio of the g_{sw} is related to AA divided by the slope:

$$-\log\left(\frac{g_{\text{sw,amphi}}}{g_{\text{sw,hypo}}}\right) = \frac{\text{AA}}{\varepsilon_g}.$$

We note that the slope in this case is an elasticity of of A to g_{sw} because both are log-transformed. This quantity will be proportional the water cost of hypostomy assuming that VPD and other environmental variables are held constant and boundary layer conductance are high enough to be negligible.

Results

Table S4: Parameter estimates and 95% confidence intervals (CIs) from the posterior distribution of the selected model. Models potentially include fixed, random, and distributional effects of growth light intensity (shade and sun), measurement light intensity (low and high), and their interaction on amphistomy advantage (AA). The distributional effects refer to the effect of factors on residual variation in AA, denoted σ, on a log-link scale. For phylogenetically structured random effects, we report the estimated standard deviation (SD).

Parameter	Estimate [95% CI]
Fixed effects	
AA intercept (shade, low light)	0.08 [0.01, 0.16]
effect of sun on AA	0.04 [-0.02, 0.12]
effect of high light on AA	-0.03 [-0.06, 0]
effect of sun $\times$ high light interaction on AA	-0.03 [-0.1, 0.03]
Distributional parameters	
$\log \sigma$ intercept (shade, low light)	-2.51 [-2.61, -2.41]
effect of sun on $\log \sigma$	0.23 [0.12, 0.33]
effect of high light on $\log \sigma$	-0.19 [-0.3, -0.09]
Random effect SDs	
AA among populations	0.06 [0.04, 0.1]
effect of sun on AA among populations	0.05 [0, 0.1]
effect of high light on AA among populations	0.02 [0, 0.05]
effect of sun $\times$ high light interaction on AA among populations	0.04 [0, 0.1]

Table S5: Parameter estimates and 95% confidence intervals (CIs) from the posterior distribution of the selected model with leaf mass per area (LMA) as potential mediator variable. Models potentially include fixed, random, and distributional effects of growth light intensity (shade and sun), measurement light intensity (low and high), log LMA, and their interactions on amphistomy advantage (AA). The distributional effects refer to the effect of factors on residual variation in AA, denoted σ, on a log-link scale. LMA can also be affected by growth light intensity and population. For phylogenetically structured random effects, we report the estimated standard deviation (SD).

Parameter	Estimate [95% CI]
Response: AA	
Fixed effects	
AA intercept (shade, low light)	-0.01 [-0.12, 0.09]
effect of sun on AA	0.01 [-0.05, 0.06]
effect of high light on AA	-0.03 [-0.07, 0]
effect of log LMA on AA	0.03 [0, 0.05]
Distributional parameters	
log σ intercept (shade, low light)	-2.5 [-2.61, -2.4]
effect of sun on log σ	0.23 [0.13, 0.34]
effect of high light on log σ	-0.19 [-0.29, -0.08]
Random effect SDs	
AA among populations	0.06 [0.04, 0.1]
effect of sun on AA among populations	0.04 [0, 0.1]
effect of high light on AA among populations	0.02 [0, 0.05]
effect of sun $\times$ high light interaction on AA among populations	0.04 [0, 0.09]
Response: log LMA	
Fixed effects	
log LMA intercept (shade)	2.99 [2.42, 3.52]
effect of sun on log LMA	0.8 [0.36, 1.27]
Random effect SDs	
log LMA among populations	0.48 [0.35, 0.66]
effect of sun on log LMA among populations	0.37 [0.23, 0.6]

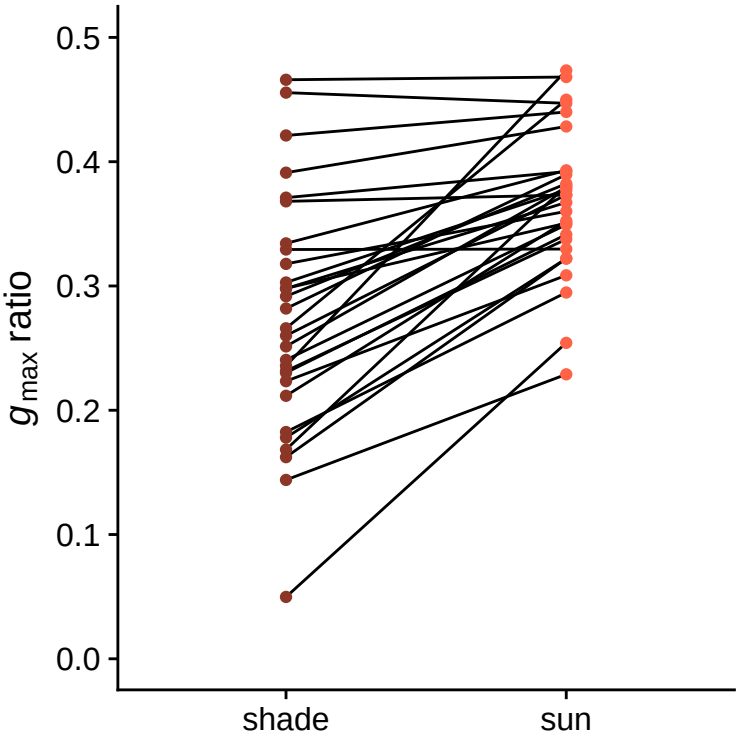

Figure S2: Developmental plasticity in anatomical maximum stomatal conductance ratio ($g_{\text{max,ratio}}$; y-axis) to growth light intensity (x-axis) among 29 wild tomato populations. All populations are amphistomatous, but vary in the stomatal density and size on each surface, which determines $g_{\text{max,ratio}}$. Each point is the average per population in that treatment; black lines connect the same population across treatments.

Table S6: Leave-one-out cross-validation information criterion (LOOIC) for models of AA as a function of light intensity, light treatment, and population. Only the top models (ΔLOOIC < 2) are shown. The model with the lowest LOOIC is considered the best fit to the data. The LOOIC column lists the LOOIC value for each model; the ΔLOOIC column lists the difference between the LOOIC of the corresponding model and the best model (lowest LOOIC). Checkmarks in each row indicate whether the corresponding model included affects of measurement light intensity ("Meas.") or growth light intensity ("Growth") as fixed effects, random effects, or distributional effect on the residual variance. We also test for fixed and random interaction effects ("Inter.") between measurement and growth light intensity. All models included phylogenetically structured random effects of population.

		Fixed			Random			Distributional	
LOOIC	ΔLOOIC	Meas.	Growth	Inter.	Meas.	Growth	Inter.	Meas.	Growth
-1882.56	0.00	✓	✓	✓	✓	✓	✓	✓	✓
-1881.70	0.86				✓	✓	✓	✓	✓
-1881.00	1.56	✓			✓	✓	✓	✓	✓
-1880.91	1.65	✓	✓		✓	✓	✓	✓	✓
-1880.63	1.93	✓	✓	✓	✓	✓		✓	✓

Table S7: Leave-one-out cross-validation information criterion (LOOIC) for models of AA as a function of light intensity, light treatment, leaf mass per area (LMA), and population. Only the top models (Δ LOOIC < 2) are shown. The model with the lowest LOOIC is considered the best fit to the data. The LOOIC column lists the LOOIC value for each model; the ΔLOOIC column lists the difference between the LOOIC of the corresponding model and the best model (lowest LOOIC). Checkmarks in each row indicate whether the corresponding model included affects of measurement light intensity ("Meas."), growth light intensity ("Growth"), or LMA as fixed or random effects. We test for fixed interaction effects between measurement and growth light intensity and LMA. We also test for random interaction effects between measurement and growth light intensity. All models included phylogenetically structured random effects of population.

		Fixed							Random		
LOOIC	ΔLOOIC	Meas.	Growth	LMA	Meas. × Growth	Meas. × Growth	Meas. × LMA	Growth × LMA	Meas.	Growth	Meas. × Growth
-1883.84	0.00	✓	✓	✓					✓	✓	✓
-1883.80	0.04	✓		✓					✓	✓	✓
-1883.67	0.17			✓					✓		
-1883.16	0.67	✓		✓					✓		
-1883.05	0.78	✓		✓				✓	✓		
-1883.05	0.78	✓		✓				✓	✓	✓	
-1882.93	0.90	✓	✓	✓		✓			✓	✓	
-1882.87	0.97	✓	✓	✓		✓			✓	✓	✓
-1882.80	1.04		✓	✓					✓	✓	✓
-1882.55	1.29	✓	✓	✓		✓			✓		
-1882.29	1.55								✓	✓	✓
-1882.27	1.56	✓	✓	✓			✓		✓	✓	✓
-1882.27	1.56	✓							✓	✓	✓
-1882.08	1.76			✓					✓	✓	✓
-1881.86	1.98	✓	✓	✓				✓	✓		

Figure S3: (Figures in separate file) The A–g_{sw} curves, fitted lines, and AA estimates for every individual plant. The title provides the Tomato Genetics Resource Center accession number, replicate letter, and species names. The subtitle indicates the growth light intensity (sun or shade). Points are raw data, lines are fitted curves, and shaded regions are 95% confidence ribbons for the fitted curves. The Bayesian correlation coefficient r^2 is shown to the right of each curve, along with the estimate of AA $\pm$ two standard errors for each pair of amphi (orange) and pseudohypo (blue) curves.